NUCLEAR STRUCTURE -- THEORY

COULOMB DISPLACEMENT ENERGY AND THE BOUND-STATE POTENTIAL FOR ^{8}B

B. A. Brown and R. Sherr[a]

Measurements of high energy solar neutrinos in the Homestake [1] and Kamiokande II and III [2] experiments have found a significantly smaller number of solar neutrinos compared to that expected from the standard solar model [3]. The ^{8}B β^+ decay is the main source of these these high energy solar neutrinos. ^{8}B is formed by the ^{7}Be(p,γ)^{8}B reaction at a center of mass energy of about 20 keV. Its cross section is conventionally expressed in terms of the S_{17} factor.[3] S_{17} is known only from an extrapolation of data at energies above 100 keV. Also the highest precision data disagree, with those of Parker [4] and Kavanagh et al.[5], being about 30 percent higher than those of Filippone et al.[6] and Vaughn et al.[7] This has lead to the investigation of other ways to determine the S_{17} factor such as the Coulomb dissociation [8], as well as other properties of ^{8}B which are indirectly related to the S_{17} factor such as its total reaction cross section [9], quadrupole moment [10], and break-up momentum distribution [11].

Much of the theoretical work has been based upon using a potential model to generate the single-particle wave function for the most loosely bound proton, and then combining this with a shell-model calculation of the spectroscopic factor to obtain the asymptotic normalization of the wave function. This current work was initiated by the observation that the potential model parameters (e.g. the radius R and diffuseness a of the Woods-Saxon potential) used in previous calculations are taken from some "standard" sets based upon nucleon-nucleus scattering optical potential analyses, and that these "standard" parameters were not obviously appropriate to the particular case of ^{7}Be plus protons. We thus investigated the extent to which the potential parameters could be determined from the displacement energy of the A=8, J^π=2^+, T=1 state as given by the binding energy difference between the ^{8}B and ^{8}Li ground states.

The relationship between the root-mean-square (rms) radius of the valence proton and the displacement energy is well known [12,13]. Qualitatively, the larger the rms radius the smaller the displacement energy since the valence proton is further from the core protons. This leads to the Thomas-Ehrman effect in which loosely bound valence nucleons have a relatively smaller displacement energy compared to more tightly bound nucleons. In addition, for a fixed binding energy, nucleons in a low ℓ state have a smaller displacement energy compared to those in a high ℓ state because the centrifugal barrier for high ℓ results in a smaller rms radius. For heavier nuclei (A>16) with a relatively simple shell-model configuration, many quantitative calculations of the displacement energy have been carried out. At the beginning of the 0d1s shell (A=17, T=1/2) and the 0f1p shell (A=41, T=1/2), the observed displacement energy is found to be about 10 percent larger than that obtained from calculations which involve only the lowest shell-model configuration together with the Coulomb interaction. These cases include those for high ℓ values whose Coulomb shift is not very sensitive to the potential-well geometry. This "Nolen-Schiffer" (NS) anomaly appears not to have a simple explanation but is due to a combination of core-polarization, high-order configuration mixing, and charge-asymmetric strong interactions effects. The systematics of the displacement energies of light nuclei can also be semi-quantitatively accounted for with a simple potential-well geometry [14].

In this study we apply what has been learned about the displacement energy systematics to constrain the shape of the potential for the ^{7}Be plus valence proton system. The A=8, T=1 displacement

energies are more complicated than the T=1/2 systems usually considered, since at least two nucleons are involved. However, the 0p shell-model wave functions predict a relatively simple structure for A=8, T=1. The spectroscopic factors (C^2S) for (A=8, 2^+, T=1) $\rightarrow$ (A=7, $3/2^-$, T=1/2) and (A=9, $3/2^-$, T=1/2) $\rightarrow$ (A=8, 2^+, T=1) are experimentally and theoretically both near unity [15,16]. Thus, ^{8}B can be considered as a proton-particle neutron-hole configuration relative to ^{8}Be. The mirror nucleus ^{8}Li is a proton-hole neutron-particle configuration. ^{8}Be is itself "deformed" and thus exits in both the ground state and 2^+ first excited state relative to the particle-hole configuration.

The displacement energy of the particle-hole state is simply the sum of the particle and hole displacement energies (the Coulomb particle-hole interaction is zero):

$$\Delta_8 = \Delta_h + \Delta_p, \tag{1}$$

where Δ_8 is the A=8, T=1 displacement energy (the binding energy difference between ^{8}Li and ^{8}B). In the simplest approximation Δ_h is the A=7, $3/2^-$, T=1/2 displacement energy and Δ_p is the A=9, $3/2^-$, T=1/2 displacement energy. The experimental values are Δ_7=1.645 MeV and Δ_9=1.851 MeV which gives $\Delta_7 + \Delta_9$=3.496 MeV compared to the experimental A=8 value of Δ_8=3.540 MeV. So the simplest model works rather well. There are however several reasons why this is not exact. One is that the actual shell-model configuration is a little more complicated than just particle-hole. Also the Thomas-Ehrman effects may be significant since the proton is unbound by by 186 keV in ^{9}B and bound by 138 keV in ^{8}B.

Since we are particularly interested in the properties of the valence proton in ^{8}B we will proceed as follows. First Eq. (1) will be modified to read

$$\Delta_8 = \Delta_h + \Delta'_p + \Delta_{sm}, \tag{2}$$

where Δ_{sm} will take into account the 0p shell-model structure beyond particle-hole. Since the hole state is relatively tightly bound, the Thomas-Ehrman shift will be small and we will take $\Delta_h = \Delta_7$ = 1.645 MeV. Δ'_p indicates the displacement energy for the particle in ^{8}B which may differ from $\Delta_p = \Delta_9$ because of the Thomas-Ehrman shift.

The shell-model correction Δ_{sm} was calculated by using the Coulomb plus charge asymmetric interaction of Ormand and Brown [17] within a full 0p shell-model basis. The matrix elements were calculated with harmonic-oscillator radial wave functions. The results for the displacement energies are: $\Delta_h = \Delta_7 = 1.719$ MeV, $\Delta_8 = 3.656$ MeV and $\Delta_p = \Delta'_p = \Delta_9 = 1.873$ MeV. This gives $\Delta_{sm} = 64$ keV. Since harmonic-oscillator radial wave functions are used the shell-model calculation should not necessarily be in good agreement with experiment, however, it should provide an estimate for the Δ_{sm} correction. Thus the displacement energy of the A=8 particle state is

$$\Delta'_p = \Delta_8 - \Delta_h - \Delta_{sm} = 1.831\,\text{MeV}. \tag{3}$$

We are interested on how Δ'_p depends upon the potential geometry, and on how the potential geometry effects the rms radius and the asymptotic density of the valence proton (which is directly related to the astrophysical S_{17} factor). To investigate this we will calculate the direct part of the Coulomb shift in a Woods-Saxon geometry. This means that we calculate the single-particle binding energy with and without the one-body Coulomb potential and take the difference to obtain the Coulomb displacement energy. The Woods-Saxons potential has the usual form of central plus spin-orbit plus Coulomb terms. The central potential has the form

$$V(r) = V_o\{1 + \exp[(r - R)/a]\}^{-1}, \tag{4}$$

where R is the radius, a is the diffuseness. We use the reduced mass in the kinetic energy operator. The spin-orbit potential is the usual derivative form with the same geometry as the central (we will show below that the spin-orbit potential is not important for our analysis). The Coulomb potential is obtained from the density distribution of four tightly-bound protons (two in 0s and two in 0p) obtained with another Woods-Saxon potential which is constrained to reproduce the experimental rms charge radius [18] of 2.52 fm for ^{9}Be.

We thus investigate the dependence of the Coulomb energy, the rms radius and the asymptotic density on the radius R and the diffuseness a of the central potential. In all cases we vary R and a and fix V_o in order to reproduce the proton separation energy of 138 keV. We calculate the direct Coulomb displacement energy Δ_o and relate it to Δ_p' by making several additional corrections, all of which are relatively small:

$$\Delta_p' = \Delta_o + \Delta_{ex} + \Delta_{so} + \Delta_{vp} + \Delta_{np} + \Delta_{NS}. \tag{5}$$

Δ_{ex} is the exchange correction. A value of Δ_{ex}=–125 keV was obtained from the harmonic-oscillator shell-model calculation for Δ_9 by comparing the results with and without the Coulomb exchange terms. The next three terms are the relativistic spin-orbit correction (Eq. 21 in Ref 12), the vacuum polarization correction (Eq. 4.23 in Ref 13) and the proton-neutron mass difference correction (Eq. 4.29 in Ref 13), respectively. Our estimates for these are −30 keV, 12 keV and 14 keV, respectively. The Nolen-Schiffer correction, Δ_{NS} is perhaps the most uncertain. For A=17 and A=41, Δ_{NS}/Δ_o is about 0.10 and we see no reason why it should differ much from this for the beginning of the 0p shell. Since Δ_o is about 1.8 MeV we will take Δ_{NS}=180 keV. Thus we arrive at the empirical value of

$$\Delta_o(\text{empirical}) = 1.780\,\text{MeV}, \tag{6}$$

with which we will compare our calculations for the direct Coulomb shift of the valence particle.

We show in Table I the results for Δ_o, the rms proton radius and the density of the valence proton at r = 10 fm, $\rho(10\,\text{fm})$, as a function of R and a. Beyond the influence of the strong interaction (about 6 fm) the shape of the radial wave function is entirely and uniquely determined by the Coulomb plus centrifugal potentials. The only quantity which depends on the potential is the asymptotic normalization as represented, for example, by the value of ρ at r = 10 fm. Our ρ(r) is defined by the normalization:

$$4\pi \int \rho(r) r^2\, dr = 1. \tag{7}$$

In order to show the correlation between Δ_o, rms and $\rho(10\,\text{fm})$ we plot values obtained for these quantities in pairs in Figs. 1 (Δ_o vs rms), 2 [Δ_o vs $\rho(10\,\text{fm})$] and 3 [rms vs $\rho(10\,\text{fm})$]. We find that there is strong correlation between them, which implies that from a knowledge of any one of them (in particular Δ_o) we can infer a range of values for the other two.

The results in Table I were obtained for a $0p_{3/2}$ valence particle. For R=2.4 fm we show the results with and without the spin-orbit potential, and from this comparison it is clear that spin-orbit potential is

Table 1: Values of Δ_o, the rms proton radius and $\rho(10\,\mathrm{fm})$ as a function of R and a.

spin-orbit	R (fm)	a (fm)	Δ_o (MeV)	rms (fm)	$\rho(10\,\mathrm{fm})\cdot 10^6$ (fm^{-3})
yes	2.0	0.4	2.108	3.70	4.25
yes	2.0	0.6	1.947	4.14	5.81
yes	2.0	0.8	1.786	4.62	8.00
yes	2.4	0.4	1.969	4.02	5.27
yes	2.4	0.6	1.840	4.40	6.85
yes	2.4	0.8	1.705	4.84	9.07
yes	2.8	0.4	1.836	4.35	6.48
yes	2.8	0.6	1.735	4.68	8.10
yes	2.8	0.8	1.623	5.08	10.40
no	2.4	0.4	1.991	3.97	5.09
no	2.4	0.6	1.851	4.38	6.74
no	2.4	0.8	1.708	4.84	9.05

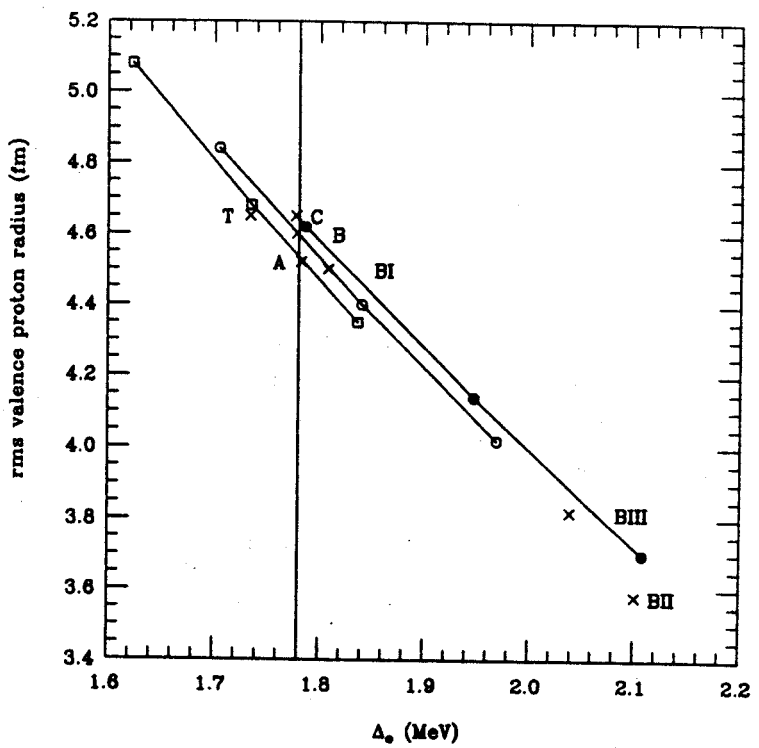

Figure 1: The valence proton rms radius as a function of Δ_o. The three lines join the points obtained for different value of the diffuseness a for R=2.0 fm (filled circles), R=2.4 fm (open circles) and R=2.8 fm (squares). The results for the specific potentials in Table II are shown by the labeled crosses.

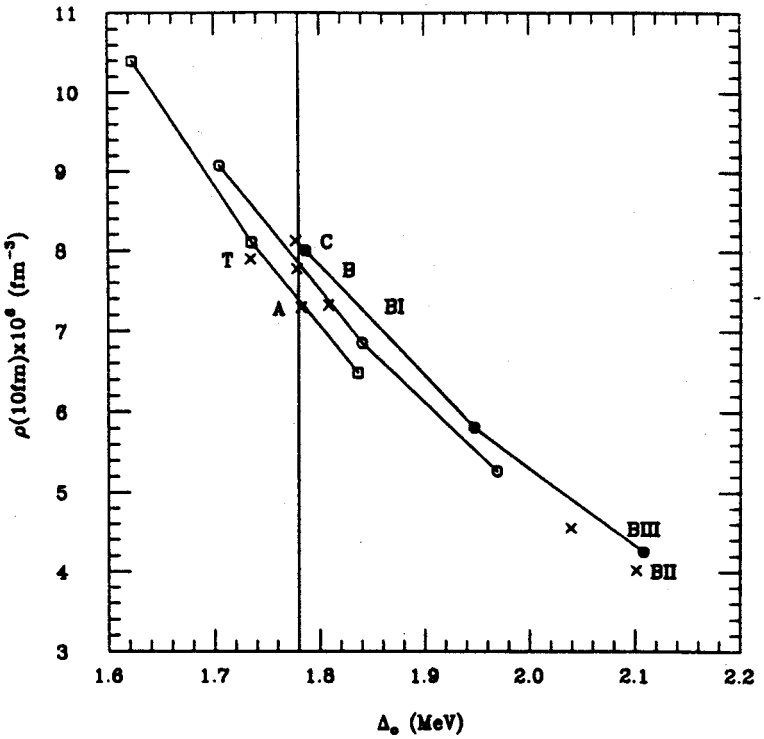

Figure 2: The valence proton density at r=10 fm as a function of Δ_o (see caption to Fig. 1).

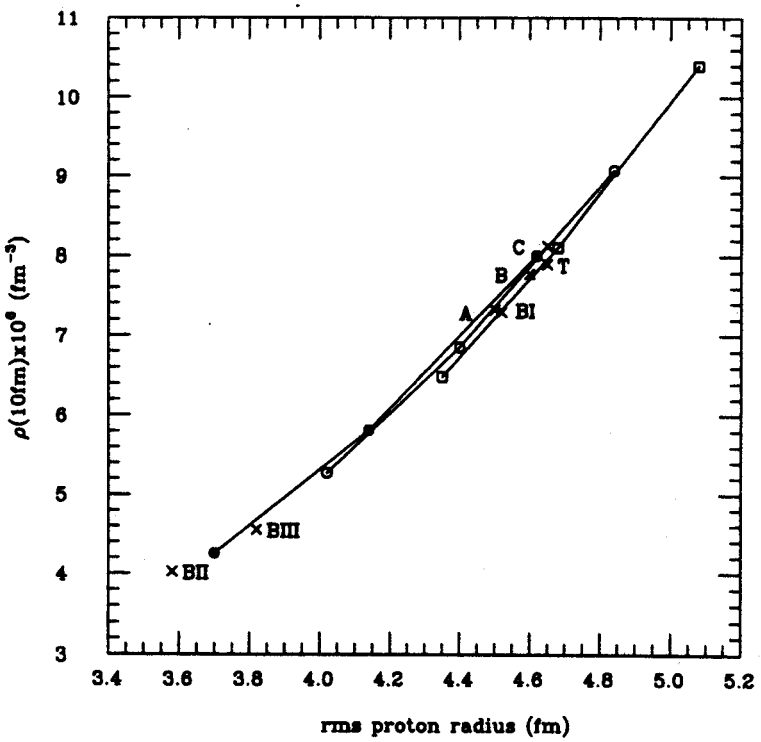

Figure 3: The valence proton density at r=10 fm as a function of the valence proton rms radius (see caption to Fig. 1).

Table 2: Woods-Saxon potential parameters from the present analysis (sets A, B and C) compared to those used by Tombrello[22] and Barker I.[23] Barker II and III correspond to those values Barker needed to reproduce the ^{7}Li(n,γ) cross section.

Set	R(fm)	a(fm)
A	2.8	0.51
B	2.4	0.69
C	2.0	0.81
Tombrello (T)	2.95	0.52
Barker BI	2.39	0.65
Barker BII	0.53	0.65
Barker BIII	2.39	0.27

not important (as long as V_o is fixed from the 138 keV separation energy). Thus to a good approximation, our results apply to both $0p_{3/2}$ and $0p_{1/2}$.

The results shown in Figs. 1–3 show that there is a rather narrow band of points which relate the quantities of interest in the framework of the Woods-Saxon potential model. From Fig. 1 one finds that the value of Δ_o=1.780 MeV corresponds to a narrow range of rms valence radii from 4.5 to 4.7 fm, and from Fig. 2 one finds that the same Δ_o corresponds to $\rho(10\,\mathrm{fm})$ values in the range 7.2 to 8.0 fm^{-3}. The correlation between the rms radius and ρ shown in Fig. 3 is even more parameter independent.

The potential parameter values required fall into three sets with (R, a) values of about (2.8, 0.51 fm) (set A), (2.4, 0.69 fm) (set B), and (2.0, 0.81 fm) (set C). Or analysis is consistent with any of these sets or any interpolation between them. These are compared in Table II to the parameters used in a number of other potential model calculations for S_{17}. The results for Δ_o, rms and $\rho(10\,\mathrm{fm})$ for the potentials in Table II are shown by the labeled crosses in Figs. 1-3. The results with Tombrello parameters (T) are close to ours. They were obtained from the optical model analysis of 180 MeV proton scattering on Li and Be by Johansson et al.[19]. The Johansson parameters were subsequently used by Aurdal [20] and Robertson [21]. Parameter set I from Barker is also close to ours. But his modifications of the parameters needed to reproduce the ^{7}Li(n,γ) cross section are clearly outside of our range.

a. Department of Physics, Princeton University, Princeton, New Jersey 08544

References

1. B. T. Cleveland, T. Daily, R. Davis, J. Distel, K. Lande, C. K. Lee, P. Wildenhain, and J. Ullman, Nucl. Phys. B (Proc. Suppl.) 38, 47 (1995).
2. Y. Suzuki, Nucl. Phys. B (Proc. Suppl.) 38, 54 (1995).
3. J. N. Bachall and R. K. Ulrich, Rev. Mod. Phys. 60, 297 (1988).
4. P. D. Parker, Phys. Rev. 150, 851 (1966).
5. R. W. Kananagh, T. A. Tombrello, T. A. Mosher and D. R. Goosman, Bull. Am. Phys. Soc. 14, 1209 (1969); R. W. Kavanagh, *Cosmology, Fusion and other Maters* (Colorado Assoc. Univ. Press, Boulder, 1972), p. 169.
6. B. W. Filippone, S. J. Elwyn, C. N. Davids and D. D. Koertke, Phys. Rev. Lett. 50, 412 (1983); Phys. Rev. C 28, 2222 (1983).
7. F. J. Vaugn, R. A. Chalmers, D. Kohler and L. F. Chase Jr., Phys. Rev. C 2, 1657 (1970).
8. T. Motobayashi et al., Phys. Rev. Lett. 73, 2680 (1994).
9. I. Tanihata et al., Phys. Rev. Lett. 55, 2676 (1985); Nucl. Phys. A520, 411c (1990); Phys. Lett. 206, 592 (1988).

10. T. Minamisono et al., Phys. Rev. Lett. 69, 2058 (1992).
11. W. Schwab et al., Z. Phys. A350, 283 (1995).
12. J. A. Nolen and J. P. Schiffer, Ann. Rev. Nucl. Sci. 19, 471 (1969).
13. S. Schlomo, Rep. Prog. Phys. 41, 957 (1978).
14. R. Sherr and G. Bertsch, Phys. Rev. C 32, 1809 (1985).
15. J. P. Schiffer, G. C. Morrison, R. H. Siemssen and B. Zeidman, Phys. Rev. 164, 1274 (1967).
16. G. B. Liu and H. T. Fortune, Phys. Rev. C 38, 1985 (1988).
17. W. E. Ormand and B. A. Brown, Nucl. Phys. A491, 1 (1989).
18. H. de Vries et al., Atomic Data and Nuclear Data Tables, 36, 3 (1987).
19. A. Johansson, U. Svandberg, and P. E. Hodgson, Ark. Fys. 19 541 (1961).
20. A. Aurdal, Nucl. Phys. A146, 385 (1970).
21. R. G. H. Robertson, Phys. Rev. C 7, 543 (1973).
22. T. A. Tombrello, Nucl. Phys. 71, 459 (1965).
23. F. C. Barker, Aust. J. Phys. 33, 177 (1980).

THE LOW-ENERGY ASTROPHYSICAL S_{17} FACTOR FOR THE ^{7}Be(p,γ)^{8}B REACTION

B. A. Brown and A. Csótó

At very low energies (< 50 keV) the ^{7}Be(p,γ)^{8}B capture cross section is dominated by the E1 transition between the ^{7}Be+p scattering states and the ^{8}B ground state [1], and it is almost exclusively determined by contributions coming form the external part of the scattering and bound state wave functions. The asymptotic behavior of the scattering states is uniquely defined (the phase shifts being the hard sphere phase shifts – practically zero), and the asymptotic part of the wave function, which describes the ^{7}Be+p relative motion in the bound state ^{8}B, is proportional to the fixed Whittaker function,

$$\psi^I_{^8\mathrm{B}}(r) = \bar{c}_I \frac{W^+_{\eta,\ell}(kr)}{r}, \quad r \to \infty, \tag{1}$$

where $I = 1, 2$ is the channel spin, r is the radial distance between ^{7}Be and p, and k is the wave number corresponding to the ^{8}B binding energy relative to the ^{7}Be+p threshold. $\bar{c}_I$ are the constants which are required to normalize the Whittaker function to the asymptotic ^{8}B wave function. Thus, at low energies the astrophysical S_{17} factor of the capture reaction,

$$S_{17}(E) = \sigma(E) E \exp\left[2\pi\eta(E)\right], \tag{2}$$

depends only on $\bar{c}[2,3]$(*here* $\eta = e^2 Z_1 Z_7/\hbar v$ with $Z_1 = 1$, and $Z_7 = 4$ is the Sommerfeld parameter). From the hard sphere scattering states one obtains:

$$S_{17}(20\mathrm{keV}) = 36.5(\bar{c}_1^2 + \bar{c}_2^2). \tag{3}$$

(The uncertainty coming mainly from the fact that the nucleon mass is not well defined in nonrelativistic quantum mechanics, is 1–2 percent. The value of the S factor at zero energy is roughly 0.4 eV-barn higher than at 20 keV.) Using this formula we can express S_{17} (in units of eV-barns) in terms of the valence proton density at any given asymptotic radius, e.g. at 10 fm,

$$S_{17}(20\,\mathrm{keV}) = 2.99{\cdot}10^6\, \rho_{3/2}(10\,\mathrm{fm})\; S_{3/2}\; [(\alpha_{1,3/2} + \gamma\,\alpha_{1,1/2})^2 + (\alpha_{2,3/2} + \gamma\,\alpha_{2,1/2})^2], \tag{4}$$

were the α coefficients are determined from the transformation between the ^{7}Be$(J_i) + \ell_j = {}^8$B(J_f) coupling and the channel-spin coupling:

$$[J_i \otimes \ell_j]^{J_f} = \sum_I \alpha_{I,j} [(J_i \otimes 1/2)^I \otimes \ell]^{J_f}, \tag{5}$$

and γ is given by the ratio:

$$\gamma = \frac{[\theta_{1/2}\; \psi_{1/2}(10\,\mathrm{fm})]}{[\theta_{3/2}\; \psi_{3/2}(10\,\mathrm{fm})]}. \tag{6}$$

In Eq. (6) θ_j is the $n = 0$, ℓ=1 spectroscopic amplitude and in Eqs. (4) S_j is the spectroscopic factor. The amplitudes θ_j are given by the reduced matrix elements [4] of the creation operator, a^+:

$$\theta_j(J_i, J_f) = \frac{\langle {}^8\mathrm{B}, J_i \,||\, a^+_{j,\mathrm{proton}} \,||\, {}^7\mathrm{Be}, J_f\rangle}{\sqrt{2J_i+1}}, \tag{7}$$

When θ_j is given without its J_i, J_f arguments as in Eq. (6), it corresponds to the ^{8}B ground state ($J_i = 2$) to ^{7}Be ground state ($J_f = 3/2$) value. The spectroscopic factors take into account the additional center of mass correction factor [5], $[A_i/(A_i-1)] = 8/7$:

$$S_j = \frac{A_i}{A_i - 1}\theta_j^2, \tag{8}$$

In Eq. (6), $\psi(10\,\mathrm{fm})$ is the radial amplitude at $r = 10$ fm:

$$\rho_j(10\,\mathrm{fm}) = \psi_j^2(10\,\mathrm{fm}). \tag{9}$$

In our case where ℓ=1, $J_i = 3/2$, $J_f = 2$ and $I = 1, 2$, the transformation coefficients are $\alpha_{1,3/2}$=$\alpha_{2,3/2}$=$\alpha_{2,1/2}$=$1/\sqrt{2}$ and $\alpha_{1,1/2}$=$-1/\sqrt{2}$. In addition, to a good approximation, $\psi_{1/2}(10\,\mathrm{fm}) = \psi_{3/2}(10\,\mathrm{fm}) = \psi(10\,\mathrm{fm})$. Hence Eq. (4) simplifies to:

$$S_{17}(20\,\mathrm{keV}) = 2.99\cdot 10^6\,\rho(10\,\mathrm{fm})\,S, \tag{10}$$

where $S = S_{3/2} + S_{1/2}$.

In Table I we give the values of θ_j obtained from 0p shell model calculations with a variety of interactions [6,7,8] which are appropriate for the lower part of the 0p shell. These amplitudes are quite stable with respect to a reasonable range of interactions.

In Table II we compare the theoretical spectroscopic factors with those obtained from reaction data [9] for states of ^{8}Li as well as those extracted from the observed widths of unbound states in ^{8}Li and ^{8}B [10]. The spectroscopic factors for the unbound states are obtained from $\Gamma_{exp} = S\,\Gamma_{sp}$ where Γ_{sp} is the single-particle width for a resonance at the experimental separation energy in the potential geometry B ($R = 2.4$ fm and $a = 0.69$ fm). The decay data are observed to be in excellent agreement with theory. The reaction spectroscopic factor for the 2^+ state is low with respect to theory, however, it depends upon the potential parameters used for the DWBA calculations (we have not attempted to repeat the DWBA calculations). The reaction spectroscopic factor for the 1^+ state is also low with respect

Table 1: Spectroscopic amplitudes $\theta_j(J_i, J_f = 3/2)$ for ^{8}B to ^{7}Be from the CKI,[6] Kumar[7] and PTBME[8] interactions. The order of the states for a given J^π_f is indicated by n_f.

J^π_f, n_f	j	CKI	Kumar	PTBME
2^+,1	3/2	0.988	0.966	0.986
	1/2	−0.237	−0.259	−0.253
1^+,1	3/2	0.567	0.606	0.552
	1/2	−0.352	−0.244	−0.342
3^+,1	3/2	0.581	0.555	0.565
1^+,2	3/2	0.617	0.574	0.525
	1/2	0.840	0.861	0.859

Table 2: Spectroscopic factors $S = S_{1/2} + S_{3/2}$ for ^{8}Li and ^{8}B.

J_f^π	$^8B_{exp}$(decay)	$^8Li_{exp}$(decay)	$^8Li_{exp}$(reaction)	CKI	Kumar	PTBME
2^+			0.87(13)	1.17	1.14	1.19
1^+	0.49(8)		0.48(7)	0.51	0.49	0.47
3^+	0.32(4)	0.38(7)		0.39	0.35	0.36

to the decay spectroscopic factor of the mirror state. The data in Table II support the 0p shell-model calculation for S and the present potential parameters. Combining with our results of $S = 1.15 \pm 0.05$ and $\rho(10\,\mathrm{fm}) = (7.7 \pm 0.4) \cdot 10^{-6}\ \mathrm{fm}^{-3}$ we obtain $S_{17}(20\,\mathrm{keV}) = 26.5 \pm 2.0$ eV-barns.

Barker [11] has pointed out that standard potential models tend to overestimate the experimentally well-determined low-energy ^{7}Li(n,γ)^{8}Li cross section. He argued, that one should modify either the potential parameters or the spectroscopic factor to get agreement with experiment. To study this issue, we performed calculations for the ^{7}Li(n,γ)^{8}Li reaction.

Because there is no Coulomb barrier in this reaction, the inner parts of the wave functions have the same importance as the asymptotic parts. Thus the cross section does not depend solely on the asymptotic normalization of the bound state wave function. For the ^{8}Li bound state we used the same potential parameters as for ^{8}B, except a change in the potential depth to get the exact neutron separation energy of 2.033 MeV. For the ^{7}Li+n scattering states, we modify the potentials to reproduce the experimental scattering lengths of the $I = 1$, and $I = 2$ channel spin states, respectively [11].

The thermal ^{7}Li(n,γ)^{8}Li cross section in our model, using potentials A, B, and C, are 78, 80 and 83 mb, respectively. The experimental thermal cross section is 45.4±3.0 mb [10]. Thus we also obtain an overestimation of the ^{7}Li(n,γ)^{8}Li cross section as did Barker. He concluded that either the potential parameters or the spectroscopic factor has to be changed in order to agree with the experiment, and that these changes would bring the ^{7}Be(p,γ)^{8}B $S_{17}(20\,\mathrm{keV})$ factor down to 16-17 eV-barns. The modifications to the potential are very large (R is changed from 2.39 to 0.53 fm or a is change from 0.65 fm to 0.27 fm) and these large changes are inconsistent with the Coulomb displacement energy analysis. Thus we can exclude the possibility of radically changing the potential parameters. In the spirit of Ref 11, the only remaining possibility would be the reduction of the spectroscopic factor to about 0.71. But given the general agreement we obtain for the decay widths in Table II, such a large change in the spectroscopic factor seems unreasonable. In fact such a drastic change would question the adequacy of the potential model itself.

We would like to point out that the discrepancy in the ^{7}Li(n,γ)^{8}Li cross section could be resolved in a way which does not affect the ^{7}Be(p,γ)^{8}B cross section. As mentioned, contrary to ^{7}Be(p,γ)^{8}B, the inner part of the wave functions is important in the case of ^{7}Li(n,γ)^{8}Li. Although the reproduction of the scattering lengths fixes the external part of the scattering wave functions, the internal, off-shell, part is not well-constrained. For instance, if the inner node of the wave function were somewhat further outside than in the potential model, this would bring the ^{7}Li(n,γ)^{8}Li cross section down. To illustrate that the node position is not well-defined, we show in Fig. 1 the inner part of the $I = 2$ scattering wave function of the standard potential (BI) of Barker [11] (solid line) together with the scattering state obtained from the cluster model of Ref 12 (dashed line) at E_{CM}=10 keV. This change in the off-shell behavior is enough to reduce the ^{7}Li(n,γ)^{8}Li cross section considerably. In fact, the dashed line of Fig. 1, together with the

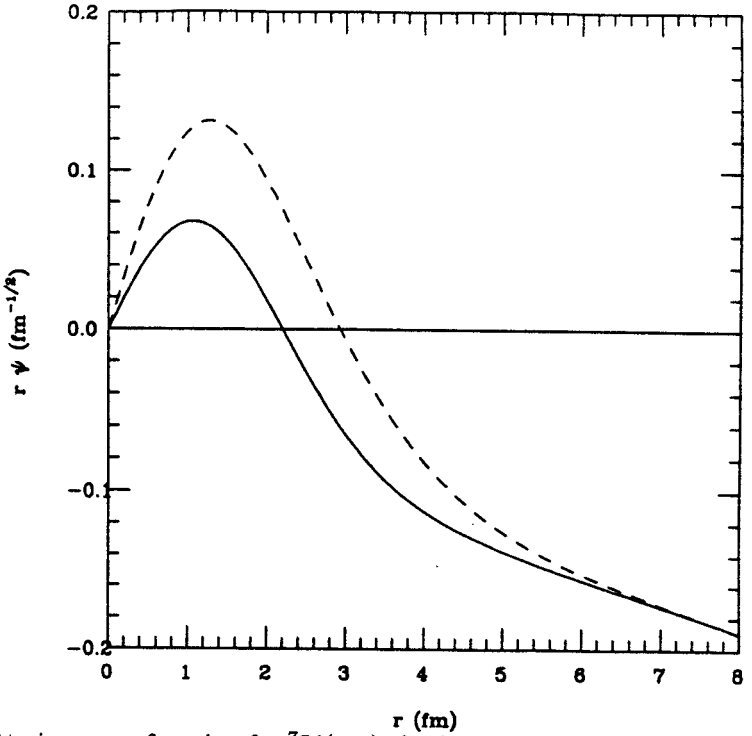

Figure 1: The scattering wave function for ^{7}Li(n,γ) obtained with the standard potential (BI) of Barker [11] (solid line) together with the results obtained with the cluster model [12] (dashed line).

bound state of the standard potential of Barker [11] results (after a $1/v$ extrapolation from 10 keV) in a thermal cross section of 46.3 mb, which is close to the experimental value. We emphasize again, that this modification in the off-shell behavior of the scattering wave functions has no effect on the ^{7}Be(p,γ)^{8}B cross section.

Our calculated value of $S_{17}(20\,\mathrm{keV}) = 26.5 \pm 2.0$ eV-barns is in agreement with the higher values of 25-27 eV-barns inferred from the (p,γ) data of Parker [13] and Kavanagh et al. [14] and is higher than the value obtained from the weighted average of all experimental data, $S_{17} = 22.2 \pm 2.3$ eV-barns [15], which is the value currently adopted in most solar models [16]. As far as other theoretical predictions are concerned, our current result for S_{17} is roughly near the highest of these (~30 eV-barns) [17] and much larger than the smallest (~17 eV-barns) [3,18].

We note, that in contrast to the common belief (e.g. Ref 18), a small value of S_{17} does not make the solar neutrino problem less severe. If one takes standard nuclear and solar physics, and standard neutrino properties, then the best fit [19] of the neutrino fluxes indicates a suppression in both the ^{7}Be (ϕ_7) and the ^{8}B (ϕ_8) neutrino fluxes, but the suppression is *much* stronger in ϕ_7. However, a smaller S_{17} value *alone* would make the predicted ϕ_7/ϕ_8 ratio larger, and hence would exagerage the solar neutrino problem.

References

1. K. H. Kim, M. H. Park, and B. T. Kim, Phys. Rev. C 35, 363 (1987).
2. R. F. Christy and I. Duck, Nucl. Phys. 24, 89 (1961); R. D. Williams and S. E. Koonin, Phys. Rev. C 23, 2773 (1981).
3. A. M. Mukhamedzhanov and N. K. Timofeyuk, JETP Lett. 51, 282 (1990); H. M. Xu, C. A. Gagliardi, R. E. Tribble, A. M. Mukhamedzhanov, and N. K. Timofeyuk, Phys. Rev. Lett. 73, 2027 (1994).
4. We use the reduced matrix element convention of A. R. Edmonds, *Angular Momentum in Quantum Mechanics*, (Princeton University Press, 1957).
5. A. E. L. Dieperink and T. de Forest, Phys. Rev. C 10, 543 (1974).
6. S. Cohen and D. Kurath, Nucl. Phys. A73, 1 (1965).

7. N. Kumar, Nucl. Phys. A235, 221 (1974).
8. R. E. Julies, W. A. Richter and B. A. Brown, S. Afr. J. Phys. 15, 35 (1992).
9. J. P. Schiffer, G. C. Morrison, R. H. Siemssen and B. Zeidman, Phys. Rev. 164, 1274 (1967).
10. F. Ajzenberg-Selove, Nucl. Phys. A490, 1 (1988); we use $\Gamma(3^+,{}^8\mathrm{Li})$=33(6) keV from Table 8.2, the $S_{exp}({}^8\mathrm{Li})$ from page 82 section 8, $\Gamma(1^+,{}^8\mathrm{B})$=37(5) keV and $\Gamma(3^+,{}^8\mathrm{B})$=350(40) keV from Table 8.9.
11. F. C. Barker, Aust. J. Phys. 33, 177 (1980).
12. A. Csótó, K. Langanke, S. E. Koonin, and T. D. Shoppa, Phys. Rev. C, in press.
13. P. D. Parker, Phys. Rev. 150, 851 (1966).
14. R. W. Kananagh, T. A. Tombrello, T. A. Mosher and D. R. Goosman, Bull. Am. Phys. Soc. 14, 1209 (1969); R. W. Kavanagh, *Cosmology, Fusion and other Maters* (Colorado Assoc. Univ. Press, Boulder, 1972), p. 169.
15. C. W. Johnson, E. Kolbe, S. E. Koonin, and K. Langanke Astrophys. J. 392, 320 (1992).
16. J. N. Bahcall and M. H. Pinsonneault, Rev. Mod. Phys. 64, 885 (1992).
17. P. Descouvemont and D. Baye, Nucl. Phys. A567, 341 (1994).
18. F. C. Barker and R. H. Spear, Astrophys. J. 307, 847 (1986); F. C. Barker, Nucl. Phys., in press (1995).
19. S. Degl'Innocenti, G. Fiorentini, and M. Lissia, preprint INFNFE-10-94, submitted to Phys. Lett. B (1994); V. Castellani, S. Degl'Innocenti, G. Fiorentini, M. Lissia, and B. Ricci, Phys. Rev. D 50, 4749 (1994); V. Castellani, S. Degl'Innocenti, G. Fiorentini, and B. Ricci, preprint, to appear in the Proceedings of the Solar Modeling Workshop, Seattle, March, 1994.

RADIAL DENSITIES AND MOMENTUM DISTRIBUTIONS FOR ^{8}B

B. A. Brown

The radial densities calculated with the potential B from the Coulomb displacement energy analysis are shown in various ways in Figs. 1-3. For the sake of simplifiction it will be assumed in this section that there is a single valence proton with a binding energy of 0.138 MeV, four tightly bound core protons (two in the 0p shell with a separation energy of about 6 MeV and two in the 0s shell with a separation energy of about 16 MeV) and three tightly bound neutrons (one on the 0p shell with a separation energy of about 8 MeV and two in the 0s shell with a separation energy of about 18 MeV). The actual situation is a little more complicated than this because $S = 1.15$ and because there is also some parentage of the protons in ^{8}B to the first excited state in ^{7}Be which will result in some leakage of the core protons to larger radii.

The normal density $\rho(r)$ is shown in Fig. 1, the probability density $P(r) = 4\pi r^2\rho(r)$ on a log scale in is shown Fig. 2, and the probability density on a linear scale is shown Fig. 3. In all figures the neutron density is shown by the dashed line, the core proton density with crosses, and the valence proton density with a solid line. Note in Figs. 2–3 that the areas are equal to three, four and one, respectively.

The valence proton (vp), core proton (cp) and neutron (n) rms radii are:

$$\sqrt{\langle r^2\rangle_{vp}} = 4.60\,\text{fm}, \tag{1}$$

$$\sqrt{\langle r^2\rangle_{cp}} = 2.39\,\text{fm}, \tag{2}$$

and

$$\sqrt{\langle r^2\rangle_{n}} = 2.21\,\text{fm}. \tag{3}$$

The total proton rms radius is given by

$$\sqrt{\langle r^2\rangle_{p}} = \sqrt{[4\langle r^2\rangle_{cp} + \langle r^2\rangle_{vp}]/5} = 2.97\,\text{fm}. \tag{4}$$

The rms charge radius includes the rms radius of 0.80 fm for the proton:

$$\sqrt{\langle r^2\rangle_{ch}} = \sqrt{[\langle r^2\rangle_{p} + 0.64\text{fm}^2]} = 3.05\,\text{fm}, \tag{5}$$

and the matter radius is given by:

$$\sqrt{\langle r^2\rangle_{m}} = \sqrt{[5\langle r^2\rangle_{p} + 3\langle r^2\rangle_{n}]/8} = 2.71\,\text{fm}. \tag{6}$$

Our results can be compared to those of other theoretical calculations. The results of $\sqrt{\langle r^2\rangle_{vp}}$ = 3.75 fm obtained by Riisager and Jensen [1] is much smaller than ours but they use an arbitrary potential shape. The calculations presented in Ref 2 for the Q moment appear to be very close to our results.

The interaction cross sections for ^{8}B and ^{8}Li on ^{12}C have been calculated with the method of Ref 3. The results with the finite-range interaction are σ=843 mb for ^{8}B and σ=820 mb for ^{8}Li. These can be compared to the experimental values of σ=784(14) mb [4] for ^{8}B and σ=768(9) mb [5] for ^{8}Li. The agreement for the magnitudes is as good as can be expected from the uncertainties in the calculation. However, the

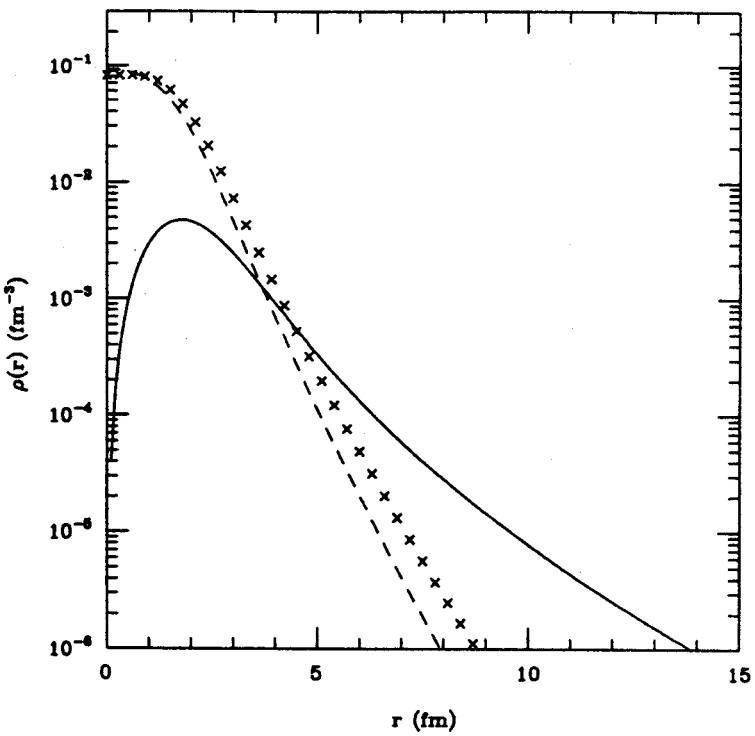

Figure 1: The radial density profile for ^{8}B for the neutrons (dashed line), the core protons (crosses) and the valence proton (solid line).

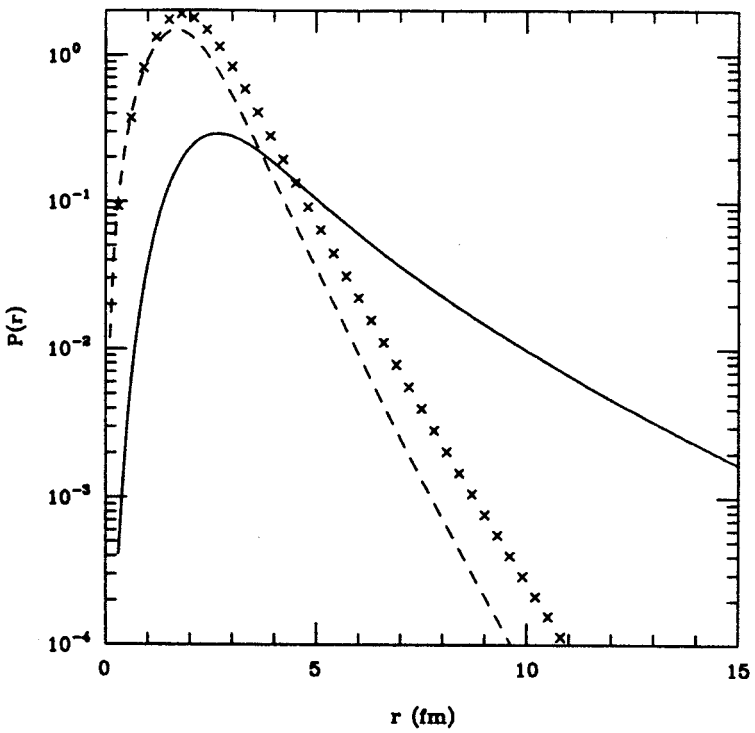

Figure 2: The radial probability distribution for ^{8}B on a log scale (see caption to Fig. 5).

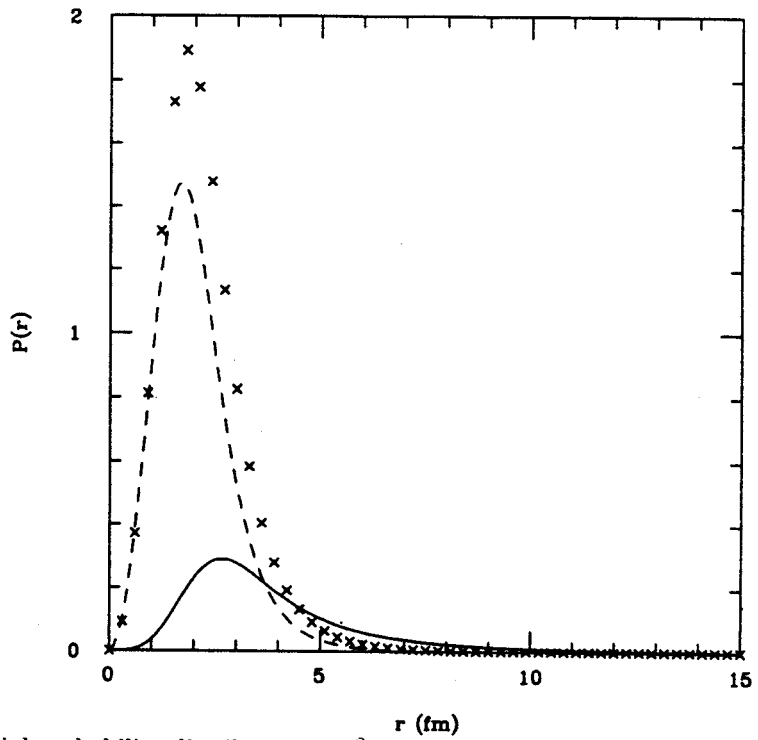

Figure 3: The radial probability distribution for ^{8}B on a linear scale (see caption to Fig. 5). The valence proton clearly has a large extension, but whether or not it constitutes a "halo" or a "skin" is a question of semantics.

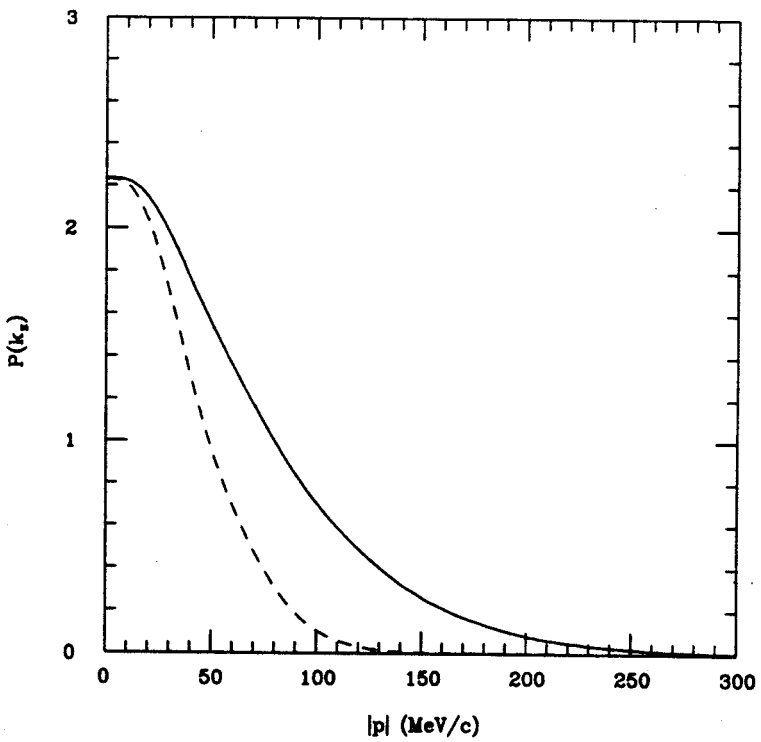

Figure 4: The momentum distribution for the ^{8}B valence proton. The solid line corresponds to the full radial wave function and the dashed line corresponds to the radial wave function cut-off at r=5 fm.

^{8}B/^{8}Li ratio (in which some of the reaction uncertainties may cancell) is in excellent agreement between theory and experiment. The effects of the proton "halo" in ^{8}B and the neutron "halo" in ^{8}Li are not large compared with the classic cases [3,5] of ^{11}Li, ^{11}Be and ^{14}Be.

Recent radiaoactive beam experiments [6,7] have looked at the momentum distribution of the ^{7}Be fragments which result from the break-up of a beam ^{8}B on various targets. From these experiments one expects to determine the momentum distribution of the most loosely bound protons. The longitudinal momemtum $P(k_z)$ obtained for the valence proton is shown in Fig. 4. This is obtained by the Fourier transform of the spacial wave function:

$$\tilde{\Psi}(\vec{k}) = \frac{1}{(2\pi)^{3/2}} \int \Psi(\vec{r}) e^{i\vec{k}\cdot\vec{r}} d^3r. \tag{7}$$

where $\Psi(\vec{r}) = \psi(r)Y_\ell(\hat{r})$, $\tilde{\Psi}(\vec{k}) = \tilde{\psi}(k)Y_\ell(\hat{k})$, and where the radial momentum distribution is given by:

$$\tilde{\psi}(k) = \sqrt{\frac{2}{\pi}} \frac{i^{-\ell}}{k} \int \psi(r) j_\ell(kr) r^2 \, dr. \tag{8}$$

The longitudinal momentum distribution is given by

$$P(k_z) = \frac{1}{2} \int \mid \tilde{\psi}(k) \mid^2 k_r dk_r, \tag{9}$$

where $k^2 = k_r^2 + k_z^2$.

The calculated momentum distribution has a width of about 150 MeV/c compared to the experimental value of 81±6 MeV/c. Given the good agreement generally found for calculated and obseved neutron halos[8] this disagreement is puzzling. There is some discussion in the literature about ways to improve the above calculation to take into account the peripheral nature of the reaction [8,9]. In the peripheral direct reaction model one puts in an additional cut-off in Eq. (9) to exclude the interior part of the radial distribution which presumably does not contribute because the cross section coming from that part is dominated by a more violent reaction where the core (^{7}Be in this case) is destroyed. We have phenomenologically modeled this effect by putting a Fermi shaped cut-off factor in Eq. (8) which has the effect of excluding the interior out to a radius R_{cut} and with a diffuseness a_{cut}. We take a_{cut}=0.65 fm and vary R_{cut} to get about the observed momentum distribtion. This requires R_{cut}=5 fm and the results are shown by the dashed line in Fig. 4. The cut-off results in a reduction of $P(k_z)$ at small momenta by a factor of 2.5 and we have renormalized the cut-off distribution by this factor in order to show the change in width. It is already known that the cut-off factor does not have much effect on the neutron halo momentum distributions [8], and we have demonstated that even a value as large as R_{cut} = 5 fm has little effect on the width of the ^{11}Be neutron halo momentum distribution. We do not know why we should need R_{cut}=5 fm, but we note that this corresponds to the point in Fig. 1–3 where the valence proton density falls below the core density. More work needs to be done to understand these results.

Schwab et al.[6] present an RPA calculation which goes beyond the 0p shell and which agrees with the shape of the observed momentum distribution. However, the shape of the wave function beyond about 6 fm as shown in Fig. 4 in their paper appears unrealistic to us. The shape beyond about 6 fm is entirely determined by the Coulomb and centrifugal barriers, and their shape differs from this expectation. Our

own calculation can of course be criticized for staying within the 0p shell. However, a very recent "no-core" calculation [10] along the lines of those given in Ref 11 which takes into account the lowest six major shells (21 shell-model orbitals) and up to $4\hbar\omega$ in excitation gives spectroscopic factors which are close to the present 0p shell results.

References

1. K. Riisger and A. S. Jensen, Phys. Lett. B 301, 6 (1993).
2. T. Minamisono et al., Phys. Rev. Lett. 69, 2058 (1992).
3. G. F. Bertsch, B. A. Brown and H. Sagawa, Phys. Rev. C 39, 1154 (1989).
4. I. Tanihata et al., Phys. Lett. B 206, 592 (1988).
5. I. Tanihata et al., Phys. Rev. Lett. 55, 2676 (1985).
6. W. Schwab et al. Z. Phys. A 350, 283 (1995).
7. J. H. Kelley et al., Bull. Am. Phys. Soc. 40, 978 (1995).
8. H. Sagawa and N. Takigawa, Phys. Rev. C 50, 985 (1994)
9. H. Sagawa and K. Yazaki, Phys. Lett. B 244, 149 (1990).
10. D. C. Zheng, B. A. Brown and B. R. Barrett, unpublished.
11. D. C. Zheng, J. P. Vary and B. R. Barrett, Phys. Rev. C 50, 2841 (1994).

QUANTUM CHAOS AND THERMALIZATION IN A FERMI SYSTEM

Mihai Horoi, Vladimir Zelevinsky and B. Alex Brown

We study the relation between the complicated structure of eigenstates in a Fermi system with strong interactions (nuclear shell model) and the general principles of statistical mechanics. The statistical approach implies that the observables are insensitive to the actual microscopic state of the system. Averaging over the equilibrium ensemble should give the same outcome as an expectation value for a typical single stationary state at the same energy. This requires the similarity of the wave functions in a given energy region which is at the same time considered as one of generic signatures of quantum chaos. In the classical case the correspondence between statistical equilibrium and chaotic trajectories exploring the whole energy surface is taken almost for granted. The definition of chaotic wave functions by Percival 1 assumes that all of them "look the same" and cover the entire available configuration space. According to Berry 2, in systems with the chaotic classical limit as a gas of hard spheres, the eigenfunctions behave like random superpositions of plane waves. This conjecture is in fact equivalent to the microcanonical ensemble and leads 3 to the standard (Maxwell-Boltzmann, Bose-Einstein or Fermi-Dirac) momentum distribution for individual particles. In self-sustained Fermi systems like nuclei, the residual interaction cannot be reduced to rare pairwise collisions and the generalization of the results derived for rigid spheres is not known.

The actual computations were performed for 12 particles in the *sd*-shell with the Wildenthal interaction 4. Many-body basis states $|k\rangle$ were constructed with good total angular momentum J and isospin T. We studied earlier 5 the signatures of quantum chaos both in energy eigenvalues and in complexity of eigenvectors. Of course, the hamiltonian matrix is far from being random since its elements are linear combinations of only few (63 in the *sd*-shell) two-body matrix elements. Eigenvalues E_α for states with $J^\pi T = 0^+0$ and 2^+0 (with model space dimensions $N = 839$ and $N = 3273$ respectively) showed perfect agreement with chaotic level statistics. The amplitudes C_k^α of eigenfunctions

$$|J^\pi T;\alpha\rangle = \sum_k C_k^\alpha |J^\pi T;k\rangle \tag{1}$$

have, for a given $|\alpha\rangle$ (except for the edges of the spectrum), Gaussian distribution with zero mean value and variance $\overline{(C_k^\alpha)^2} = 1/N^\alpha$. The localization length N^α gives a measure of complexity of the eigenstates at energy E_α. In the extreme chaotic case N^α approaches the dimension N manifesting total mixing and delocalization of eigenfunctions. The information entropy,

$$S^\alpha = -\sum_k (C_k^\alpha)^2 \ln[(C_k^\alpha)^2], \tag{2}$$

as well as moments of the distribution function of the components C_k^α, show that, as the excitation energy increases, the eigenfunctions become more complex and the maximum of complexity is reached in the middle of the spectrum. Our measures of complexity are basis dependent. We argued 5, 6 that the mean field basis is preferential for such an analysis.

The same process of stochastization can be described in the basis-independent thermodynamic language. The statistical weight $\Omega(E) = \rho(E)\Delta E$ determines microcanonical entropy $S^{th}(E) = \ln \Omega(E)$ and

temperature T according to

$$\frac{\partial S^{th}}{\partial E} = \frac{1}{T}. \tag{3}$$

For 0^+0 states, the level density $\rho(E)$ presented as a histogram in Fig. 1a together with a Gaussian fit with the centroid at $E_0 = -90MeV$ and variance $\sigma_E = 13$ MeV. The temperature $T = \sigma_E^2/(E_0 - E)$ is shown by a solid line in Fig. 1*b*. The right half of the spectrum is associated with decreasing entropy and negative temperature.

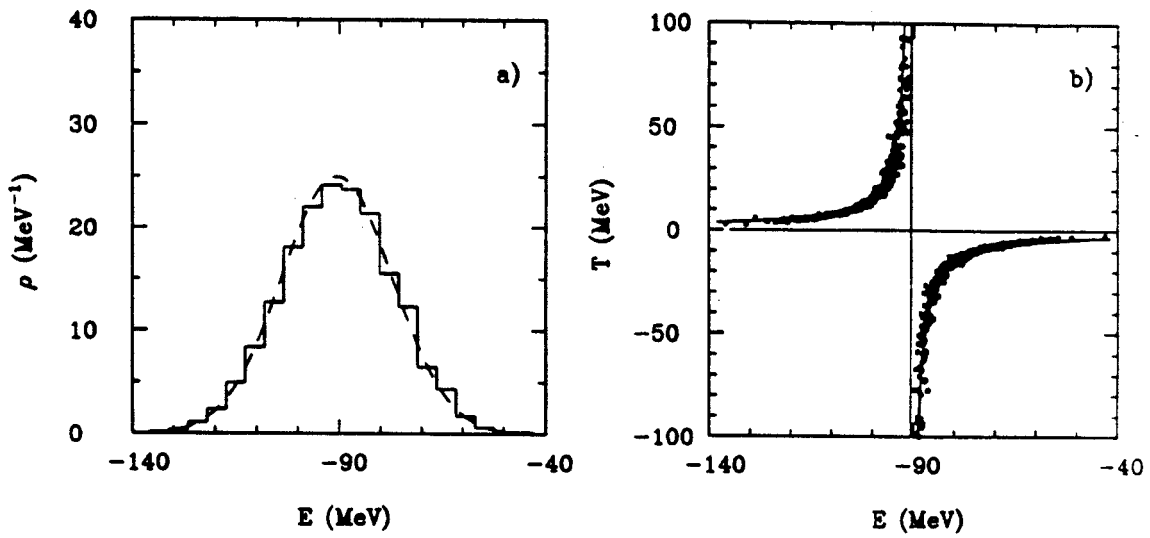

Figure 1: Level density $\rho(E)$ for 0^+0 states (panel a), a histogram is compared with the Gaussian fit (dashed line); panel *b*: temperature calculated from the global fit to the level density (solid line) and found from the occupation numbers of Fig. 2a (dots).

Fig.2 shows the single-particle occupation numbers n_λ^α of the orbitals $\lambda = (l, j)$ for many-body states $|\alpha\rangle$, eq.(1). The panels *a*,*b* and *c* correspond to $0^+0, 2^+0$ and 9^+0 $(N = 657)$ states, respectively.

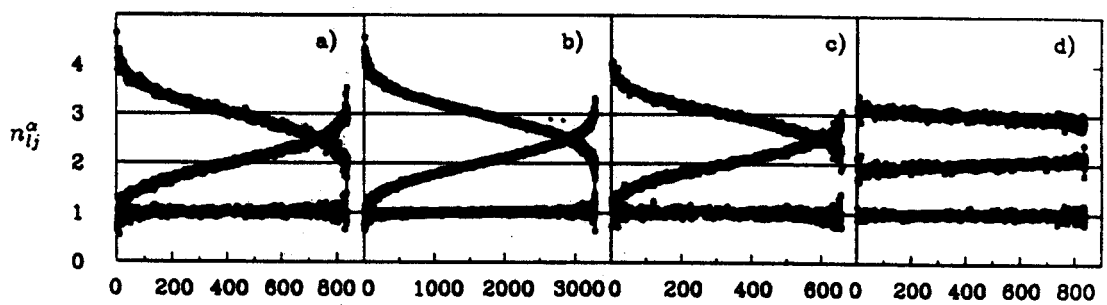

Figure 2: Single-particle occupation numbers, eq.(4), *vs* state number α for states 0^+0 (panel a), 2^+0 (panel *b*), and 9^+0 (panel *c*). Panel *d* shows occupation numbers for 0^+0 states for diagonal matrix elements reduced by a factor 10. For all panels the three curves (sets of points) refer to $s_{1/2}, d_{3/2}$ and $d_{5/2}$ orbitals, from bottom to top.

All classes exhibit an identical smooth behavior of n_λ^α. It suggests that one can associate to each eigenstate $|\alpha\rangle$ a single-particle "temperature" T_{s-p}^α defined by the Fermi distribution $f_{lj}^\alpha = \{\exp[(e_{lj} - \mu)/T_{s-p}^\alpha] + 1\}^{-1}$. In the center of the spectrum (infinite temperature) all occupancies $f_{lj}^\alpha = n_{lj}^\alpha/(2j+1)$

are equal the common value being 1/2 for our case of 12 particles in the sd-shell. The effective energies $e_{lj} - \mu$ are -3.4, 0.0 and 4.7 MeV for $d_{5/2}, s_{1/2}$ and $d_{3/2}$ orbitals respectively (for comparison, the shell model spin-orbit splitting near the ground state is 7.2 MeV). One can then extract the T^{α}_{s-p} for each level $|\alpha\rangle$, Fig. 1b (dots), and check that the "single-particle thermometer" on average measures the same temperature as obtained from the level density. The system can be considered as an equilibrated Fermi-liquid and its properties can be expressed in terms of occupation numbers for interacting quasiparticles.

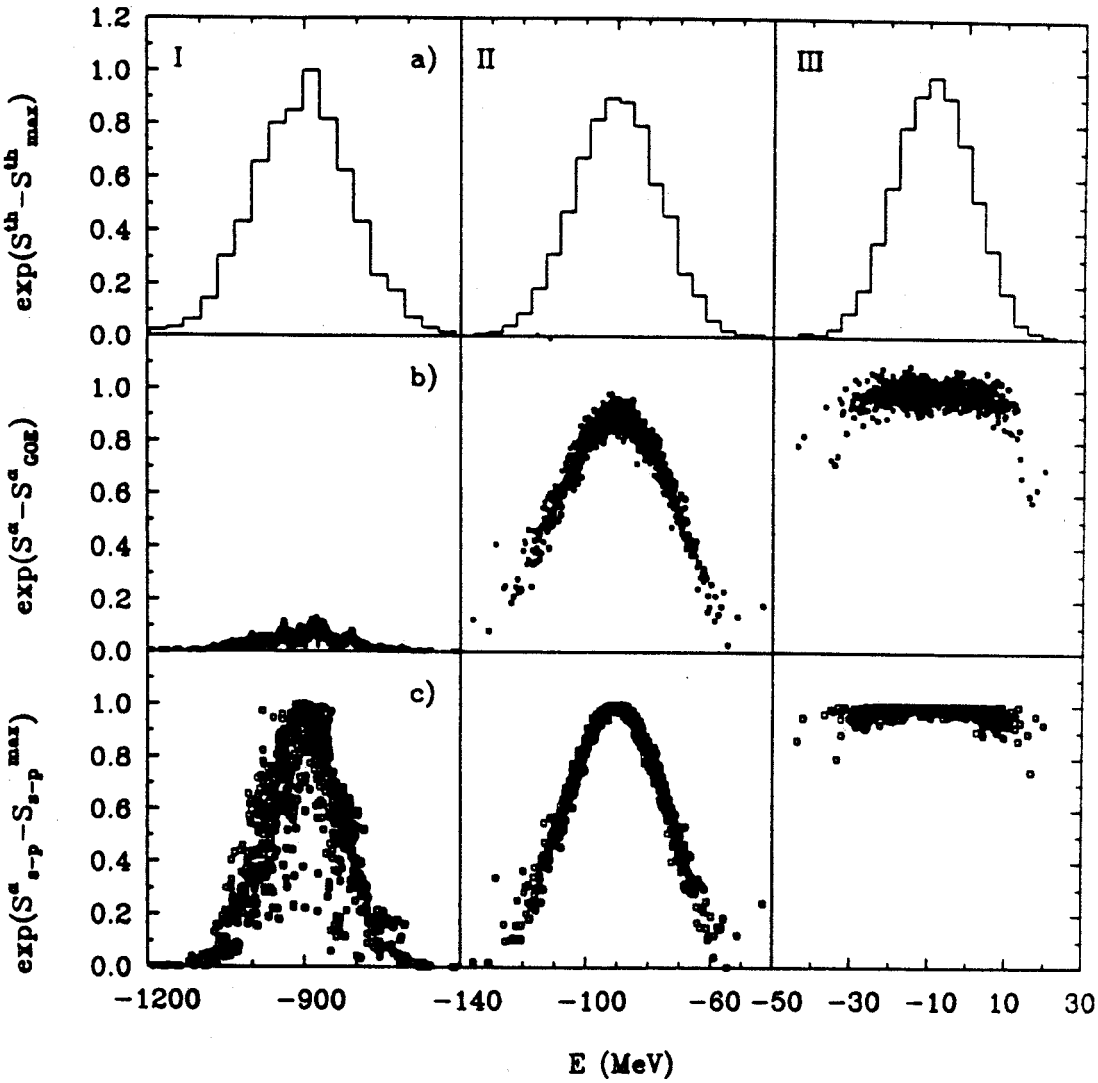

Figure 3: Entropy-like quantities plotted as a function of energy for 0^+0 states. Columns correspond to the diagonal matrix elements multiplied by factors of 10 (I), 1 (II) and 0.1 (III), the latter case coincides with that of Fig. 2d. Rows a, b and c correspond to total statistical weight $\Omega(E)$ in units of the weight for the middle of the spectrum; informational entropy, eq.(2), of individual states in units of the GOE entropy for the complete mixing, $\exp(S^{\alpha}_{GOE}) = 0.48N$; and single-particle entropy, eq.(5), of individual states calculated from the occupation numbers, in units of $S^{max}_{s-p} = 2^{24}$, respectively.

Using the occupancies f^{α}_{lj} of individual orbitals one can calculate the single-particle entropy of the

quasiparticle gas for each state $|\alpha\rangle$,

$$S^{\alpha}_{s-p} = -\sum_{lj\tau}(2j+1)[f^{\alpha}_{lj}\ln f^{\alpha}_{lj} + (1-f^{\alpha}_{lj})\ln(1-f^{\alpha}_{lj})]. \quad (4)$$

Now we have three entropy-like quantities: thermodynamic entropy $S^{th}(E) \sim \ln\rho(E)$, information entropy S^{α} (2) and single-particle entropy S^{α}_{s-p} (4), the latter two for individual eigenstates. In Fig. 3 we juxtapose $\exp(S)$ for different situations.

Rows a,*b* and *c* present S^{th}, S^{α} and S^{α}_{s-p}, respectively, for 0^+0 states. The column I shows the limit of weak off-diagonal interaction. The thermodynamic entropy I*a* displays Gaussian behavior of a combinatorial nature. Within the fluctuations, it is similar to the single-particle picture I*c*. The information entropy I*b* is low; only at high level density does one see some mixing. This is an equilibrium picture of almost non-interacting particles where the degree of complexity is only weakly correlated with thermalization. Using the language of kinetic theory, collisions (mixing) are necessary for equilibration but the equilibrium properties do not depend on the collision rate.

The opposite case III (and Fig. 2*d*) corresponds to strong off-diagonal interaction. The states are strongly mixed and the information entropy III*b* is near its chaotic maximum 5 of $\exp(S^{\alpha})_{chaotic} = 0.48N = 404$ for 0^+0 states. S^{α}_{s-p} (III*c*) is also at the maximum level corresponding to the equiprobable population of orbitals. Within the fluctuations, S^{α} and S^{α}_{s-p} coincide. However, as seen from III*a*, the system has normal thermodynamic properties governed by the level density. Whence, in the absence of the (diagonal) mean field the response to thermal excitation cannot be expressed in terms of quasiparticles. The interaction is too strong and the mixing does not depend on the actual level spacing. Almost all wave functions "look the same" regardless of level density and the quasiparticle "thermometer" cannot resolve the spectral regions with different temperatures. In both cases, I and III, the information entropy becomes irrelevant for thermodynamics although it still characterizes degree of complexity of eigenstates in the mean field basis.

The case of the realistic mean field and empirical residual interaction is shown in column II. With the normalized magnitudes, all three entropies are identical within fluctuations except for the edges of the spectrum. For the majority of states and for the mean field consistent with residual interactions, the thermodynamic entropy defined either via the global level density or in terms of occupation numbers behaves similar to the information entropy.

One can conclude that (i) equilibrium heating is strongly correlated with the evolution of many-body chaos and increase of complexity of individual eigenstates; (ii) equilibrium properties of a heated system with strong interactions can still be described in terms of quasiparticles and their effective energies in the appropriate mean field.

References

1. I.C.Percival, J. Phys. B6, L229 (1973).
2. M.V.Berry, J. Phys. A10, 2083 (1977).
3. M.Srednicki, Phys. Rev. E50, 888 (1994).
4. B.A.Brown and B.H.Wildenthal, Ann. Rev. Nucl. Part. Sci. 38, 29 (1988).
5. V.Zelevinsky, M.Horoi and B.A.Brown, Phys. Lett. B (1995), in press.
6. V.G.Zelevinsky, Nucl. Phys. A555, 109 (1993).

CHAOTIC DYNAMICS AND COLLECTIVE STRENGTH FUNCTIONS

Vladimir Zelevinsky

The relaxation of collective modes is recognized by the width Γ of the strength function $P(E)$. Part of it Γ_0 arises from the decay into compound states. Some conclusions concerning this damping width can be made based on the chaotic character of many-body dynamics 1.

The mean field hamiltonian generates the shell structure. Its eigenstates are the independent many-particle many-hole excitations. They are strongly mixed by the residual interaction V. The resulting picture of dense spectrum and complicated eigenstates, analyzed in the realistic shell model 2, exhibits generic features of quantum chaos. Simple states $|k\rangle$ are fragmented over many eigenstates $|\alpha\rangle$. This spreading is described by a set of uncorrelated amplitudes, $|k\rangle = \sum_\alpha C_k^\alpha |\alpha\rangle$. The associated strength function is

$$P_k(E_\alpha) = \rho(E_\alpha)|\langle k|\alpha\rangle|^2 = \rho(E_\alpha)|C_k^\alpha|^2, \tag{1}$$

where ρ denotes the total density of states with the same quantum numbers. The strength functions are normalized according to $\int dE_\alpha P_k(E_\alpha) = 1$.

Using the arguments developed within the context of rotational damping 3 we assume the *uniformity*: generic states $|k\rangle$ are all characterized by a single strength function P centered around each unperturbed energy E_k so that $P_k(E_\alpha) = P(E_\alpha - E_k)$, where we imply averaging over some nearby states $|k\rangle$. The strength function $P_0(E - E_0)$ of the collective state $|0\rangle$ can be exceptional because of its highly coherent character 4. Therefore we allow the strength function P_0 to be different from P.

In the shell model the mixing starts with the "doorway" states. The uniformity assumption requires that the coupling between the states $|k\rangle$ have a uniform distribution. For the average coupling strength per unit energy,

$$\rho_k(E_l)\overline{|H_{kl}|^2} = f(E_k - E_l), \tag{2}$$

Here ρ_k denotes the level density of those states which couple, through the interaction V, to a given state $|k\rangle$. Similarly, for the giant resonance state $|0\rangle$,

$$\rho_0(E_k)\overline{|H_{0k}|^2} = f_0(E_k - E_0), \tag{3}$$

with ρ_0 being the density of doorway states for the collective excitation $|0\rangle$.

The diagonalization of the full Hamiltonian H now proceeds in two steps. First H is diagonalized among all the states $|k\rangle$ except for the single state $|0\rangle$, thus producing a new set of eigenstates $|q\rangle$. These states $|q\rangle$ have no mutual interactions but couple to the state $|0\rangle$ with matrix elements

$$\overline{|H_{0q}|^2} = \overline{|\sum_k H_{0k}\langle k|q\rangle|^2} \approx \sum_k \overline{|H_{0k}|^2}\,\overline{|\langle k|q\rangle|^2} \approx \sum_k \overline{|H_{0k}|^2}\,\frac{1}{\rho(E_k)} P_k(E_q). \tag{4}$$

Here we assumed that 1) the amplitudes are uncorrelated, 2) the omission of the state $|0\rangle$ does not affect the strength function $P_k(E)$.

The second part of the diagonalization can be carried out exactly, with the strength function given by

$$P_0(E-E_0) = \frac{1}{\pi}\mathrm{Im}\,[E-E_0-\Sigma_0(E-E_0)]^{-1},$$

$$\Sigma_0(E-E_0) = \sum_q \frac{|H_{0q}|^2}{E-E_q-i0}. \qquad (5)$$

Averaging over nearby shell model states, we find

$$\Sigma_0(E-E_0) = \int dx \int dy\, f_0(x-y)\,\frac{P(y)}{E-E_0-x-i0}. \qquad (6)$$

Equations (5-6) relate the strength function P_0 of the collective state to the strength function P of the states $|k\rangle$.

One can use the same procedure of two-step diagonalization for any state $|k\rangle$ to substitute the infinite set of equations for P_k by the integral equation for the common strength function $P(E)$,

$$P(z) = \frac{1}{\pi}\mathrm{Im}\,[z-\Sigma(z)]^{-1},$$

$$\Sigma(z) = \int dx \int dy\, f(x-y)\,\frac{P(y)}{z-x-i0}. \qquad (7)$$

The set of eqs. (5-7) contains the coupling of the collective excitation to a hierarchy of complicated states. In shell model calculations the equations are truncated at a maximum number of particle-hole excitations. Here instead, the strength functions for high seniority states are not neglected but rather retained at a limiting form. The formfactor f_0 depends both on the strength $n_0v_0^2$ (in terms of a typical r.m.s. matrix element v_0 and the number of doorway states n_0) as well as the energy range W_0 of the residual interaction. The corresponding quantities for a generic state are nv^2 and W. As the excitation energy (temperature) increases, the number of doorway states increases while the average coupling decreases so that the combinations $n_0v_0^2$ and nv^2 remain essentially constant ($\sqrt{N}$-scaling 5).

In the weak coupling limit, $\sqrt{n_0}v_0 \ll W_0$ and $\sqrt{n}v \ll W$, the self-energy $\Sigma_0(z)$ is a slowly changing function of energy within the spreading width. Consequently, the collective strength function $P_0(E-E_0)$ will not depend on the details of $P(x)$ and eventually attain a Breit-Wigner form (exponential decay) with the golden rule spreading width

$$\Gamma_0 = 2\,\mathrm{Im}\Sigma_0(0) = 2\pi v_0^2\rho_0(E_\mu \approx E_0) = 2\pi f_0(0) = \frac{4n_0v_0^2}{W_0};\quad \sqrt{n_0}v_0 \ll W_0. \qquad (8)$$

This relation applies if Γ_0 is much smaller than the range of the interaction W_0.

In the strong coupling limit, $\sqrt{n}v \gg W$, the exact shape of the coupling is not important. The self-consistent strength function of background states is a semicircle,

$$P(z) = \frac{2}{\pi R^2}\sqrt{R^2 - z^2}, \quad R = 2\sqrt{n}v; \quad \sqrt{n}v \gg W. \tag{9}$$

The collective strength function becomes

$$P_0(z) = \frac{2}{\pi}\frac{\sqrt{R^2 - z^2}}{R_0^2 + 4z^2(R^2/R_0^2 - 1)}, \tag{10}$$

where $R_0 = 2\sqrt{n_0}v_0$, that is, a hybride of the semicircle and Breit-Wigner shapes. The effective spreading width (FWHM) of the collective resonance varies from $\Gamma_0 = \sqrt{3}R_0$ at $R_0 = R$ to $\Gamma_0 = R_0^2/R$ at $R \gg R_0$. The upper boundary for the width is determined solely by the coupling to the doorway states. Subsequent scattering may change the shape of the strength function but does not add to the damping width which may actually decrease due to the effect similar to motional narrowing 3,6. The limiting forms are valid only for the central part of the strength function; its wings depend on the details of the energy dependence of the coupling matrix elements.

R_0 is proportional to $\sqrt{\langle 0|H^2|0\rangle}$ and does not contain any exponentially growing parameters. Since $\sqrt{3}R_0$ provides an upper bound for the damping width, Γ_0 does not increase indefinitely with temperature but saturates at a modest value, determined by the properties of the residual interaction between simple states. Experimental studies of the properties of the GDR in hot nuclei seem to give support to these results 7.

Another example is provided by isobaric analog resonances. The variations of the spreading width of IAR are small 8. In this case the residual interaction mixes the resonance with the background states of lower isospin. The ratio $\Gamma^{\downarrow}/v_0$ gives a measure of the isospin violation which is a smooth function of A 9. Recent data for the isospin mixing in light nuclei (A$\approx$ 60) 10, show that the width $\Gamma^{\downarrow}$ remains constant even at excitation energies $\sim$100 MeV, where the evaporation width is much larger than $\Gamma^{\downarrow}$.

In conclusion, the damping width of a collective vibration does not depend on the detailed coupling to the compound states. For chaotic intrinsic dynamics, the width is not sensitive to the temperature and at most is equal to few times a typical matrix element of the residual interaction mixing mean field configurations.

References

1. B.Lauritzen, P.F.Bortignon, R.A.Broglia and V.G.Zelevinsky, Preprint NBI-94-56.
2. V. Zelevinsky, M. Horoi and B. A. Brown, *to be published.*
3. B. Lauritzen, T. Døssing and R. A. Broglia, Nucl. Phys. A457, 61 (1986).
4. G. F. Bertsch, P. F. Bortignon and R. A. Broglia, Rev. Mod. Phys. 55, 287 (1983).
5. O. P. Sushkov and V. V. Flambaum, Sov. J. Nucl. Phys. 33, 31 (1981); Sov. Phys. Usp. 25, 1 (1982).
6. R. A. Broglia, T. Døssing, B. Lauritzen and B. R. Mottelson, Phys. Rev. Lett. 58, 326 (1987).
7. R. A. Broglia, P. F. Bortignon and A. Bracco, Progr. Part. Nucl. Phys. 28, 527 (1992); P. F. Bortignon *et al.*, Phys. Rev. Lett. 67, 3360 (1991).
8. J. Reiter and H. L. Harney, Z. Phys. A337, 121 (1990).
9. V. G. Zelevinsky and P. von Brentano, Nucl. Phys. A529, 141 (1991).
10. J. A. Behr *et al.*, Phys. Rev. Lett. 70, 3201 (1993); K. A. Snover, Nucl. Phys. A553, 153c (1993), Fig.6.

"SIGN PUZZLE" IN PARITY VIOLATING NEUTRON SCATTERING FROM ^{232}Th

Vladimir Zelevinsky

Large effects of parity nonconservation (PNC) in compound nuclear states 1, 2 are observed in experiments with polarized neutrons. The mechanism of statistical enhancement due to the high level density 3, 4, 5 is considered to be responsible for the large magnitude of the effects. The enhancement in comparison to the parity mixing between single-particle states is proportional to $\sqrt{N}$ where $N \sim 10^5 - 10^6$ is a number of shell model configurations in a compound wave function. Matrix elements of the weak interaction H_W between compound states of opposite parity are suppressed by a factor $\sim 1/\sqrt{N}$ but the level spacing is diminished by a factor $\sim N$. Additional enhancement due to the interference of s- and p- wave neutron resonances mixed by weak interaction is provided4 by the factor $(\Gamma_s^{(n)}/\Gamma_p^{(n)})^{1/2} \sim 1/kR \sim 10^2 - 10^3$ where k is neutron wave number, R is nuclear radius, $\Gamma_s^{(n)}$ and $\Gamma_p^{(n)}$ are neutron widths for the s- and p-waves, respectively. Acting together, those factors enhance the difference of total cross sections $\sigma_\pm$ for neutrons with positive and negative helicity so that the observed asymmetry

$$P = \frac{\sigma_+ - \sigma_-}{\sigma_+ + \sigma_-} \tag{1}$$

reaches in some cases the magnitude of about 10%.

Statistical nature of the enhancement implies randomness of matrix elements of weak interaction between complicated states of opposite parity. Therefore one would expect the random sign of asymmetry (1). Recent LAMPF experiments 2 show the same sign for all eight statistically significant p-resonances in ^{233}Th. Other compound nuclei seem to be closer to the random distribution of the sign. In all cases the order of magnitude of the effect agrees with the predictions based on the two enhancement factors. Several attempts to find a mechanism generating a regular component of the PNC asymmetry were unsuccessful in the sense that the desired magnitude of the weak matrix elements was inconsistent with our knowledge on weak interactions in nuclei.

The new idea 6 relates the experimental pattern for Th with pecularities of its structure as compared to "normal" deformed nuclei like ^{238}U which apparently exhibit random asymmetry. Th isotopes display strong octupole correlations 7, 8. At energies near neutron threshold, the nuclear wave function has a significant probability of large octupole deformation, $\beta_3 \simeq 0.35$.

In neutron capture by a spinless target the states have the angular momentum projection onto the symmetry axis $|K| = 1/2$. For a given intrinsic function $|a\rangle$ with $K \neq 0$, the presence of any shape which is axially symmetric but has no symmetry with respect to reflection in the equatorial plane, leads to rotational doublets with definite parity η,

$$|\Psi^I_{MK;\eta}\rangle = \sqrt{\frac{2I+1}{8\pi}}\{D^I_{MK}(\varphi,\theta,0)|a;K\rangle + \eta(-1)^{I+K}D^I_{M-K}(\varphi,\theta,0)|a;-K\rangle\}. \tag{2}$$

Energy splitting of doublet states implies that there exist a physical interaction (like Coriolis force or cluster tunneling) which can couple "right- and left- oriented" configurations $|a;\pm K\rangle$. For the doublet energy separation of the order of several keV, the mixing by weak interaction of the doublet states would be much more favorable than the mixing of the single-particle orbitals separated by MeV. However, the direct

mixing of states (2) with the same intrinsic structure and opposite η is forbidden if the weak perturbation H_W does not violate time reversal symmetry along with space inversion symmetry 9.

The mixing of the doublet states by the P-odd T-even interaction should be mediated by another ("normal", P- and T-even) interaction H' leading to the admixtures of different configurations $|b;K'\rangle$. It can (but does not have to) be the same interaction which splits the doublet. H' influences PNC via the P-conserving mixing matrix element

$$\langle \Psi^{aI}_{MK;\eta}|H'|\Psi^{bI}_{MK;\eta}\rangle = \eta A_{IK}\langle a;-K|H'|b;K\rangle \tag{3}$$

with the amplitude A_{IK} depending on the nature of H'. As a result of the joint action of H' and H_W the total function (1) acquires an admixture of opposite parity,

$$|\Psi^{aI}_{MK;\eta}\rangle \to |\tilde{\Psi}^{aI}_{MK;\eta}\rangle = |\Psi^{aI}_{MK;\eta}\rangle + \beta|\Psi^{aI}_{MK;-\eta}\rangle. \tag{4}$$

The mixing amplitude

$$\beta = -2\eta\frac{A_{IK}}{E-E_{-\eta}}\sum_b \frac{\langle a;-K|H'|b;K\rangle\langle b;K|H_W|a;K\rangle}{E-E_b} \tag{5}$$

is directly related to the observed PNC asymmetry (1), $P = 2\sqrt{\Gamma^{(n)}_s/\Gamma^{(n)}_p}\beta$, where the ratio of widths gives the kinematic enhancement.

If the splitting of the doublet is due to the same interaction H' it also can be expressed in terms of the amplitude A_{IK}. Assuming that the product of matrix elements in eq.(5) is peaked for the states b on the distance $E_b - E \simeq \omega$ from the resonance, the closure approximation gives

$$\beta = \frac{\langle a;-K|H'H_W|a;K\rangle}{\omega\langle a;-K|H'|a;K\rangle}. \tag{6}$$

Thus, in this scheme one can expect the admixture amplitude of the order $\beta \simeq (H_W)_{s-p}/\omega$ where $(H_W)_{s-p}$ is given by the typical single-particle matrix elements of weak interaction, $(H_W)_{s-p} \simeq 5$ eV. For the Coriolis force as H', the transition energy between deformed single-particle orbitals with $\Delta m = \pm 1$ is of the order of 100 keV which leads to the estimate $\beta \simeq 5\times 10^{-5}$. As a result, the regular component gives the observed effect of $P \simeq 10^{-2}$.

This can be compared with the mixing between compound states of opposite parity where $\beta_{comp} \simeq \langle H_W\rangle_{comp}/D$. The experimental data 2 show that $\langle H_W\rangle_{comp} \approx 1.3\times 10^{-3}$ eV. Using this value and $D = 15$ eV, we obtain $\beta_{comp} \simeq 10^{-4}$.

For a P- and T-odd interaction, direct mixing within the doublet is not forbidden which can be of some interest for the problem of search for $T-$ and P-violating nuclear forces. In this respect the situation is similar to that in the problem of the electric dipole moment of a particle.

References

1. V.P.Alfimenkov *et al.*, Pis'ma Zh. Exptl. Theor. Fiz. 34, 308 (1981) [JETP Lett. 34, 295 (1981)]; Nucl. Phys. A398, 93 (1983); Usp. Fiz. Nauk 144, 361 (1984) [Sov. Phys. Usp. 27, 797 (1984)].

2. J.D.Bowman *et al.*, Phys. Rev. Lett. 65, 1192 (1990); C.M.Frankle *et al.*, Phys. Rev. Lett. 67, 564 (1991).
3. R.J.Blin-Stoyle, Phys. Rev. 120, 181 (1960).
4. O.P.Sushkov and V.V.Flambaum, Pis'ma Zh. Exptl. Theor. Fiz. 32, 377 (1980) [JETP Lett. 32, 353 (1980)]; Usp. Fiz. Nauk 136, 3 (1982) [Sov. Phys. Usp. 25, 1 (1982)]; Nucl. Phys. A412, 13 (1984).
5. N.Auerbach and B.A.Brown, Phys. Lett. B340, 6 (1994).
6. V.V.Flambaum and V.G.Zelevinsky, Phys. Lett. B (1995) in press.
7. G.A.Leander *et al.*, Nucl. Phys. A388, 452 (1982).
8. W.Nazarewicz, Nucl. Phys. A520, 333c (1990).
9. O.P.Sushkov, V.V.Flambaum, Yad.Fiz. 31, 55 (1980) [Sov.J. Nucl.Phys. 31, 28 (1980)].